Strojniški vestnik - Journal of Mechanical Engineering 59(2013)5, 291-300
DOI:10.5545/sv-jme.2012.727
Original Scientific Paper
Received for review: 2012-08-06
Received revised form: 2012-10-11
Accepted for publication: 2013-02-14

Analysing Kinematics of a Novel 3CPS Parallel Manipulator Based on Rodrigues Parameters

Gang Cheng[1,*] – Peng Xu[1] – De-hua Yang[2] – Hui Li[2] – Hou-guang Liu[1]

[1] China University of Mining and Technology, College of Mechanical and Electrical Engineering, China
[2] Chinese Academy of Sciences, National Astronomical Observatories, Nanjing Institute of Astronomical Optics and Technology, China

In order to adjust the poses of the segment mirrors and give the correct surface shape to a large aperture telescope, an active adjusting platform for segment mirror with a novel 3CPS parallel manipulator as core module is proposed. The platform has 6 degree-of-freedoms (DOFs) including three translational freedoms and three rotational freedoms. Its kinematics are analysed systematically. By means of the Rodrigues parameters method, the formulae for solving the inverse/forward displacement, the inverse/forward velocity, and the inverse/forward acceleration kinematics are derived. A numerical simulation of the kinematics model is then carried out combining the topological structure characteristics of the manipulator. The correctness of the kinematics model is verified by an experiment in which the pose of moving platform is measured using a photogrammetric method.

Keywords: active adjusting platform, 3CPS parallel manipulator, Rodrigues parameters, kinematics, photogrammetry

0 INTRODUCTION

Astronomy seeks the detection of more distant and dim celestial bodies. Large aperture optical systems are significant in astronomy research for their increased light gathering capability and angular resolution in the object space [1]. Therefore, the development of telescopes with large apertures and high imaging quality is necessary. However, as the size of the telescopes increases, they become increasingly sensitive to external disturbances such as thermal gradients, gravity, and wind, and also to internal disturbances from support equipment such as pumps, cryocoolers, and fans [2]. In order to decrease these influences, most large aperture telescopes in the future will be segmented [3], such as the US/Japanese Thirty Meter Telescope and the European-ELT 42m telescope projects. For these telescopes, the large aperture primary mirrors are spliced by many small aperture and thin segment mirrors. The advantages of this approach, where the mass and size of the primary mirror are no longer the main factors affecting the observation results, are obvious. However, comparing the telescope with one entire primary mirror, the main problems with this approach are the position and orientation disorders of the segment mirrors. The development of an active adjusting mechanism for a large number of mirrors with multiple degrees of freedom is urgent.

In recent years, parallel manipulators have seen growing applications in robotics, machine tools, positioning systems, measurement devices, and so on [4] to [8]. The classic 6 DOFs parallel manipulator (Stewart platform) has many characteristics, such as simple structure, concise principle, flexible function, high accuracy, and high stiffness. It has also been used in the field of astronomical telescope and instruments [9] to [11]. However, the six driving legs of the Stewart platform have strong coupling movements and the distance between the moving platform and fixed base is usually large. These shortcomings, as well as the structure type of the Stewart platform, are not suitable for making large-scale active adjustments in compact spaces. In order to overcome the defects mentioned above, an active adjusting platform prototype of a segment mirror with a novel 3CPS parallel manipulator as the core module is proposed. The parallel manipulator is composed of a moving platform, a fixed base and three CPS chains, where the notation CPS denotes the kinematic chain made up of a cylindrical joint, a prismatic joint, and a spherical joint in series.

Kinematic analysis is a common basis of dynamic analysis and control system design. The kinematics of parallel manipulators includes inverse kinematics and forward kinematics. Numerous researchers have made contributions to this. Cheng et al. [12] studied the inverse/forward displacement, velocity, and acceleration kinematics of a 3SPS+1PS bionic parallel test platform by means of the unit quaternion method. Lu et al. [13] studied kinematics, statics, and workspaces of a 3R1T 4 DOFs and a 1R3T 4 DOFs parallel manipulators, comprehensively. Gallardo et al. [14] studied the kinematics of modular spatial hyper-redundant manipulators formed from RPS-type limbs based on screw theory and recursive method. Cui et al. [15] analysed the kinematics of a TAU parallel manipulator based on a D-H model and solved

*Corr. Author's Address: China University of Mining and Technology, College of Mechanical and Electrical Engineering, 221008, Xuzhou, China, chg@cumt.edu.cn

its forward kinematics in closed forms by a Jacobian approximation method. Varedi et al. [16] analysed the kinematics of an offset 3UPU translational parallel manipulator by the homotopy continuation method, which alleviates the drawbacks of traditional numerical techniques, namely: the acquirement of good initial guess values, the problem of convergence, and computing time. The main research methods of kinematics can be divided into analytical and numerical ones. For the parallel manipulators whose structures are not complex, the analytical method can solve the kinematics competently and solution procedures can be fully automated. For parallel manipulators with complex structures, the analytical method is always inadequate and the obtained solutions can be too complex to subsequently analyse. The computational accuracy and speed of the numerical method depend on the complexity of mechanisms and algorithms themselves whose flexibility and portability is quite often poor. Due to the simple mechanical structure, the analytical method is adopted to analyse the kinematics in this paper.

The rest of the paper is organized as follows: In section 1, the structure of the active adjusting platform prototype is described and the reference systems of the manipulator are established. In section 2, the inverse/forward displacement, the inverse/forward velocity, and the inverse/forward acceleration kinematics of the manipulator are studied based on the Rodrigues parameters. In section 3, a numerical simulation of the kinematics analysis is conducted, and lastly the numerical results are validated by experiments.

1 DESCRIPTION OF 3CPS PARALLEL MANIPULATOR

The active adjusting platform for the segment mirror considered in this paper is shown in Fig. 1a and the topological structure of its core module, a 3CPS parallel manipulator, is shown in Fig. 1b. Taking the 3CPS parallel manipulator as an analysis object, reference systems for kinematic analysis are established. The absolute coordinate system $\{B\}$ is fixed on B at point O. The Y-axis of $\{B\}$ passes through point A_2, the Z-axis is perpendicular to B pointing to m. The X-axis can be determined by the other two axes following the right-hand-rule (RHR). Three vertical legs with cylindrical joints (C_i, i =1, 2, 3) are installed symmetrically about point O on B. Every mount point is equidistant from point O and the distance denotes as E. Three horizontal legs with prismatic joints (P_i, i = 1, 2, 3) are fixed on the end points of three vertical legs (D_i, i = 1, 2, 3). They rotate around Z-axis in the same direction and the angles between the horizontal legs and the corresponding sides of triangular B are equal. Three equal-length short legs are connected to the horizontal legs and the lengths were unchanged. In the following analysis, the lengths of the short legs can add to the lengths of the vertical legs. The short legs are connected to m with sphere joints (S_i, i = 1, 2, 3). The distances of mount points in m are equal to each other. The relative coordinate system $\{m\}$ is attached to m at point o. The y-axis of $\{m\}$ passes through point a_2, the z-axis is perpendicular to m pointing upward. The x, y and z axis follow the RHR. Three spherical joints are installed on m and the distance from mount point to point o is denoted as e. When the length of the vertical legs are equal, namely: $h_i = h_0$ (i = 1, 2, 3) and the length of the horizontal legs are equal, namely: $l_i = l_0$ (i = 1, 2, 3), the manipulator is at the equilibrium position.

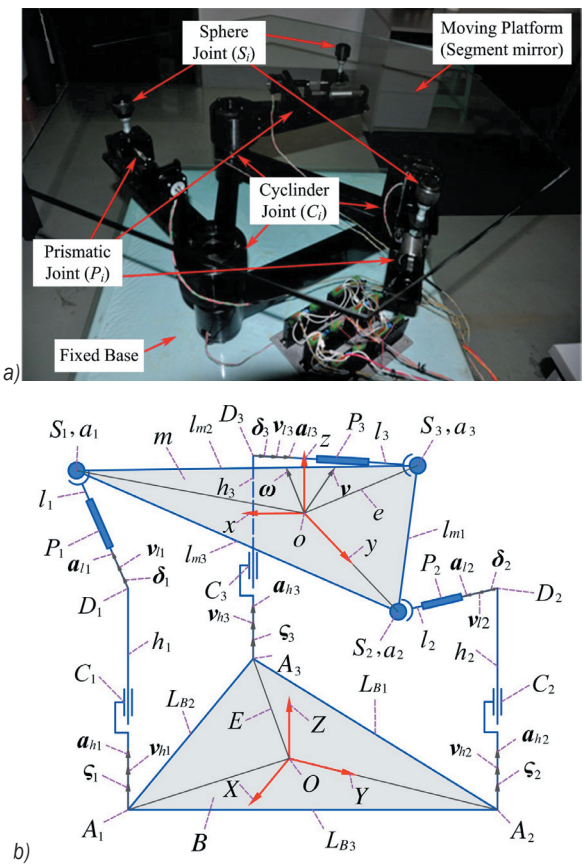

Fig. 1. *The 3CPS parallel manipulator; a) a prototype of the active adjusting platform, and b) the topological structure of the active adjusting platform*

This prototype has partial DOF-decoupling motion characteristics. The rotations around the X-axis, Y-axis and the translations along the Z-axis are driven by the three vertical leg h_i (i = 1, 2, 3),

while the translations along the *X*-axis, the *Y*-axis and the rotations around *Z*-axis are driven by the three horizontal legs l_i (i = 1, 2, 3), respectively.

When the manipulator is at the equilibrium position, the moving platform is parallel to the fixed base. Let θ be the rotational angle around the *Z*-axis between the moving platform and the fixed base. According to the cosine formula, the formula for solving θ is expressed as:

$$\theta = arc\cos(\frac{E^2 + e^2 - l_0^2}{2Ee}). \quad (1)$$

Using a Kutzbach Grübler equation [17], the DOF of 3CPS parallel manipulator is calculated as:

$$F = 6\left(n - g - 1\right) + \sum_{i=1}^{g} f_i = 6, \quad (2)$$

where, F is the DOF of the manipulator, n is the number of components, g is the number of kinematics pairs, and f_i is the degree of freedom of the i^{th} kinematics pair. It can be seen clearly that the parallel manipulator has 6 DOFs including three translational freedoms and three rotational freedoms.

2 MANIPULATOR KINEMATICS ANALYSES

2.1 Inverse/Forward Displacement Analysis

Before analysing the kinematics of 3CPS manipulator, the coordinates of the points A_i (i = 1, 2, 3) in $\{B\}$ and the coordinates of the points a_i (i = 1, 2, 3) in $\{m\}$ and $\{B\}$ must be determined. They are expressed as:

$$\boldsymbol{A}_i^B = \begin{bmatrix} X_{Ai} \\ Y_{Ai} \\ Z_{Ai} \end{bmatrix}, \quad \boldsymbol{a}_i^m = \begin{bmatrix} x_{ai} \\ y_{ai} \\ z_{ai} \end{bmatrix}, \quad \boldsymbol{a}_i^B = \begin{bmatrix} X_{ai} \\ Y_{ai} \\ Z_{ai} \end{bmatrix},$$

$$\boldsymbol{o}^B = \begin{bmatrix} X_o \\ Y_o \\ Z_o \end{bmatrix}, \quad \boldsymbol{a}_i^B = \boldsymbol{D}_o \boldsymbol{a}_i^m + \boldsymbol{o}^B, \quad (3)$$

where, $\boldsymbol{o}^B$ is a vector of point o on m in $\{B\}$, (X_o, Y_o, Z_o) are the components of $\boldsymbol{o}^B$, $\boldsymbol{D}_o$ is a rotation transformation matrix from $\{m\}$ to $\{B\}$ based on Rodrigues parameters and it can be written as follows [18]:

$$\boldsymbol{D}_o = \begin{bmatrix} x_l & y_l & z_l \\ x_m & y_m & z_m \\ x_n & y_n & z_n \end{bmatrix} = \frac{1}{\lambda_0^2} \begin{bmatrix} 1+\Phi_1^2-\Phi_2^2-\Phi_3^2 & 2\left(\Phi_1\Phi_2-\Phi_3\right) & 2\left(\Phi_1\Phi_3+\Phi_2\right) \\ 2\left(\Phi_2\Phi_1+\Phi_3\right) & 1-\Phi_1^2+\Phi_2^2-\Phi_3^2 & 2\left(\Phi_2\Phi_3-\Phi_1\right) \\ 2\left(\Phi_3\Phi_1-\Phi_2\right) & 2\left(\Phi_3\Phi_2+\Phi_1\right) & 1-\Phi_1^2-\Phi_2^2+\Phi_3^2 \end{bmatrix}, \quad (4)$$

where, $\lambda_0^2 = 1 + \Phi_1^2 + \Phi_2^2 + \Phi_3^2$ and (x_l, x_m, x_n, y_l, y_m, y_n, z_l, z_m, z_n) are the nine orientation parameters of m in $\{B\}$.

By rotation transformation, the absolute coordinates $\boldsymbol{a}_i^B$ of the point a_i (i = 1, 2, 3) can be derived from Eqs. (3) and (4). The absolute coordinates $\boldsymbol{D}_i^B$ of the point D_i (i = 1, 2, 3) can be expressed as follows:

$$\boldsymbol{D}_i^B = \boldsymbol{A}_i^B + \boldsymbol{R}\boldsymbol{a}_i^B, \quad (5)$$

where, $\boldsymbol{R}$ = [0 0 0; 0 0 0; 0 0 1].

According to the formula of distance between two spatial points, the length of the vertical leg h_i (i = 1, 2, 3) and the horizontal leg l_i (i = 1, 2, 3) can be derived as follows:

$$h_i = \sqrt{\left(\boldsymbol{D}_i^B - \boldsymbol{A}_i^B\right)^{\mathrm{T}} \left(\boldsymbol{D}_i^B - \boldsymbol{A}_i^B\right)},$$
$$l_i = \sqrt{\left(\boldsymbol{a}_i^B - \boldsymbol{D}_i^B\right)^{\mathrm{T}} \left(\boldsymbol{a}_i^B - \boldsymbol{D}_i^B\right)}. \quad (6)$$

The unit vector $\boldsymbol{\varsigma}_i$ along the vertical legs h_i, the unit vector $\boldsymbol{\delta}_i$ along the horizontal legs l_i and the vector $\boldsymbol{e}_i$ of line oa_i can be expressed as:

$$\boldsymbol{\varsigma}_i = \frac{\boldsymbol{D}_i^B - \boldsymbol{A}_i^B}{h_i}, \quad \boldsymbol{\delta}_i = \frac{\boldsymbol{a}_i^B - \boldsymbol{D}_i^B}{l_i}, \quad \boldsymbol{e}_i = \boldsymbol{a}_i^B - \boldsymbol{o}^B. \quad (7)$$

The unit vector $\boldsymbol{\xi}_i$ is the tangent vector of the horizontal legs l_i rotating around vertical legs h_i and can be expressed as follow:

$$\boldsymbol{\xi}_i = \boldsymbol{\delta}_i \times \boldsymbol{\varsigma}_i. \quad (8)$$

When given three Rodrigues parameters Φ_i (i = 1, 2, 3) and $\boldsymbol{o}^B$, the inverse displacement parameters (h_i, l_i, $\boldsymbol{\varsigma}_i$, $\boldsymbol{\delta}_i$, $\boldsymbol{e}_i$, i = 1, 2, 3) can be solved from Eqs. (6) and (7). When given the lengths of the six input driving legs h_i (i = 1, 2, 3) and l_i (i = 1, 2, 3), from Eq. (6), the position and orientation parameters of moving platform can be obtained by solving a nonlinear kinematic equations system.

2.2 Inverse/forward Velocity and Jacobian Matrix

Let $\boldsymbol{V}$ be the general velocity of m at point o and $\boldsymbol{v}$ be the linear velocity, while $\boldsymbol{\omega}$ is the angular velocity of m at point o and $\boldsymbol{v}_i$ is a linear velocity of m at point a_i. Let $\boldsymbol{v}_h$ and $\boldsymbol{v}_l$ be the input velocities of vertical legs and horizontal legs, respectively. This can be expressed as follows:

$$\boldsymbol{V}=\begin{bmatrix}\boldsymbol{v}\\ \boldsymbol{\omega}\end{bmatrix}_{6\times1},\quad \boldsymbol{v}=\begin{bmatrix}v_1\\ v_2\\ v_3\end{bmatrix},\quad \boldsymbol{\omega}=\begin{bmatrix}\omega_1\\ \omega_2\\ \omega_3\end{bmatrix},$$
$$\boldsymbol{v}_i=\boldsymbol{v}+\boldsymbol{\omega}\times\boldsymbol{e}_i,\quad \boldsymbol{v}_h=\begin{bmatrix}v_{h1}\\ v_{h2}\\ v_{h3}\end{bmatrix},\quad \boldsymbol{v}_l=\begin{bmatrix}v_{l1}\\ v_{l2}\\ v_{l3}\end{bmatrix}. \tag{9}$$

Let $\boldsymbol{u}_o$, $\boldsymbol{v}_o$ and $\boldsymbol{w}_o$ be the unit vectors of x, y and z axes of the moving platform in $\{B\}$, respectively. These expressions can be obtained by rotation transformation from $\{m\}$ to $\{B\}$:

$$\boldsymbol{u}_o=\boldsymbol{D}_o\begin{bmatrix}1\\0\\0\end{bmatrix},\quad \boldsymbol{v}_o=\boldsymbol{D}_o\begin{bmatrix}0\\1\\0\end{bmatrix},\quad \boldsymbol{w}_o=\boldsymbol{D}_o\begin{bmatrix}0\\0\\1\end{bmatrix}. \tag{10}$$

The angular velocity $\boldsymbol{\omega}$ of m at point o can be expressed as follows:

$$\boldsymbol{\omega}=\boldsymbol{u}_o\omega_1+\boldsymbol{v}_o\omega_2+\boldsymbol{w}_o\omega_3. \tag{11}$$

The ω_1, ω_2 and ω_3 are the components of $\boldsymbol{\omega}$ and can be obtained by dot-multiplying Eq. (11) with $(\boldsymbol{v}_o\times\boldsymbol{w}_o)$, $(\boldsymbol{u}_o\times\boldsymbol{w}_o)$ and $(\boldsymbol{u}_o\times\boldsymbol{v}_o)$ at both sides, respectively:

$$\omega_1=\frac{(\boldsymbol{v}_o\times\boldsymbol{w}_o)\cdot\boldsymbol{\omega}}{(\boldsymbol{v}_o\times\boldsymbol{w}_o)\cdot\boldsymbol{u}_o},\quad \omega_2=\frac{(\boldsymbol{u}_o\times\boldsymbol{w}_o)\cdot\boldsymbol{\omega}}{(\boldsymbol{u}_o\times\boldsymbol{w}_o)\cdot\boldsymbol{v}_o},$$
$$\omega_3=\frac{(\boldsymbol{u}_o\times\boldsymbol{v}_o)\cdot\boldsymbol{\omega}}{(\boldsymbol{u}_o\times\boldsymbol{v}_o)\cdot\boldsymbol{w}_o}. \tag{12}$$

According to the geometrical characteristics of the manipulator, the linear velocity $\boldsymbol{v}_{hi}$ along vertical legs h_i (i = 1, 2, 3) and the linear velocity $\boldsymbol{v}_{li}$ along horizontal legs l_i (i = 1, 2, 3) can be obtained from Eq. (9) and can be expressed as follows:

$$v_{hi}=\boldsymbol{v}_i\cdot\boldsymbol{\varsigma}_i=\begin{bmatrix}\boldsymbol{\varsigma}_i^{\mathrm{T}} & \left(\boldsymbol{e}_i\times\boldsymbol{\varsigma}_i\right)^{\mathrm{T}}\end{bmatrix}\boldsymbol{V}, \tag{13a}$$

$$v_{li}=\boldsymbol{v}_i\cdot\boldsymbol{\delta}_i=\begin{bmatrix}\boldsymbol{\delta}_i^{\mathrm{T}} & \left(\boldsymbol{e}_i\times\boldsymbol{\delta}_i\right)^{\mathrm{T}}\end{bmatrix}\boldsymbol{V}. \tag{13b}$$

By combining Eq. (13a) and Eq. (13b), the formulae for solving the inverse/forward velocities can be obtained and expressed as follows:

$$\begin{bmatrix}v_{h1}\\ v_{h2}\\ v_{h3}\\ v_{l1}\\ v_{l2}\\ v_{l3}\end{bmatrix}=\boldsymbol{J}\boldsymbol{V},\quad \boldsymbol{J}=\begin{bmatrix}\boldsymbol{\varsigma}_1^{\mathrm{T}} & \left(\boldsymbol{e}_1\times\boldsymbol{\varsigma}_1\right)^{\mathrm{T}}\\ \boldsymbol{\varsigma}_2^{\mathrm{T}} & \left(\boldsymbol{e}_2\times\boldsymbol{\varsigma}_2\right)^{\mathrm{T}}\\ \boldsymbol{\varsigma}_3^{\mathrm{T}} & \left(\boldsymbol{e}_3\times\boldsymbol{\varsigma}_3\right)^{\mathrm{T}}\\ \boldsymbol{\delta}_1^{\mathrm{T}} & \left(\boldsymbol{e}_1\times\boldsymbol{\delta}_1\right)^{\mathrm{T}}\\ \boldsymbol{\delta}_2^{\mathrm{T}} & \left(\boldsymbol{e}_2\times\boldsymbol{\delta}_2\right)^{\mathrm{T}}\\ \boldsymbol{\delta}_3^{\mathrm{T}} & \left(\boldsymbol{e}_3\times\boldsymbol{\delta}_3\right)^{\mathrm{T}}\end{bmatrix}_{6\times6}, \tag{14}$$

where, $\boldsymbol{J}$ is a velocity Jacobian matrix.

From Eqs. (8) and (9), the formulae for solving the tangential velocities of the horizontal legs at point a_i when rotating around the vertical legs are expressed as:

$$v_{ti}=\boldsymbol{v}_i\cdot\boldsymbol{\xi}_i=\begin{bmatrix}\boldsymbol{\xi}_i^{\mathrm{T}} & \left(\boldsymbol{e}_i\times\boldsymbol{\xi}_i\right)^{\mathrm{T}}\end{bmatrix}\boldsymbol{V}. \tag{15}$$

From Eqs. (6) and (15), the angular velocities ω_{Ci} of the vertical legs are derived as shown below:

$$\omega_{Ci}=\frac{v_{ti}}{l_i},\quad (i=1,2,3). \tag{16}$$

2.3 Inverse/forward Acceleration and Hessian Matrix

First, a skew symmetric matrix is briefly introduced. Suppose two vectors $\boldsymbol{\mu}$ and $\boldsymbol{\nu}$ and a skew symmetric matrix $S(\boldsymbol{\mu})$ for $\boldsymbol{\mu}$:

$$\boldsymbol{\mu}=\begin{bmatrix}\mu_x\\ \mu_y\\ \mu_z\end{bmatrix},\boldsymbol{\nu}=\begin{bmatrix}\nu_x\\ \nu_y\\ \nu_z\end{bmatrix},S(\boldsymbol{\mu})=\begin{bmatrix}0 & -\mu_z & \mu_y\\ \mu_z & 0 & -\mu_x\\ -\mu_y & \mu_x & 0\end{bmatrix}. \tag{17}$$

Eq. (17) satisfies the following relationships [19]:

$$\boldsymbol{\mu}\times\boldsymbol{\nu}=S(\boldsymbol{\mu})\cdot\boldsymbol{\nu}=-S(\boldsymbol{\nu})\cdot\boldsymbol{\mu},$$
$$S(\boldsymbol{\mu})^{\mathrm{T}}=-S(\boldsymbol{\mu}),$$
$$-S(\boldsymbol{\mu})^2+S(\boldsymbol{\mu})\cdot S(\boldsymbol{\mu})^{\mathrm{T}}=\mathbf{I}_{3\times3}, \tag{18}$$

where, $\mathbf{I}_{3\times3}$ is an order 3 unit matrix.

Let $\boldsymbol{A}$ be the general acceleration of m at point o, where $\boldsymbol{a}$ and $\boldsymbol{\varepsilon}$ are the linear and angular acceleration of m at point o, respectively. Let $\boldsymbol{a}_h$ and $\boldsymbol{a}_l$ be the input accelerations of the vertical legs and the horizontal legs, respectively. They can be expressed as follows:

$$\boldsymbol{A}=\begin{bmatrix}\boldsymbol{a}\\ \boldsymbol{\varepsilon}\end{bmatrix},\quad \boldsymbol{a}=\begin{bmatrix}a_x\\ a_y\\ a_z\end{bmatrix},\quad \boldsymbol{\varepsilon}=\begin{bmatrix}\varepsilon_x\\ \varepsilon_y\\ \varepsilon_z\end{bmatrix},$$
$$\boldsymbol{a}_h=\begin{bmatrix}a_{h1}\\ a_{h2}\\ a_{h3}\end{bmatrix},\quad \boldsymbol{a}_l=\begin{bmatrix}a_{l1}\\ a_{l2}\\ a_{l3}\end{bmatrix}. \tag{19}$$

By differentiation of Eq. (13a) with respect to time, the acceleration $\boldsymbol{a}_{hi}$ along the i^{th} vertical leg is derived as below:

$$a_{hi}=\begin{bmatrix}\boldsymbol{\varsigma}_i^{\mathrm{T}} & \left(\boldsymbol{e}_i\times\boldsymbol{\varsigma}_i\right)^{\mathrm{T}}\end{bmatrix}\boldsymbol{A}+\begin{bmatrix}\boldsymbol{0}_{1\times3} & \left(\dot{\boldsymbol{e}}_i\times\boldsymbol{\varsigma}_i\right)^{\mathrm{T}}\end{bmatrix}\boldsymbol{V},\quad (i=1,2,3), \tag{20a}$$

where,

$$\left(\dot{\boldsymbol{e}}_i\times\boldsymbol{\varsigma}_i\right)^{\mathrm{T}}=\left[-S\left(\boldsymbol{\varsigma}_i\right)\left(\boldsymbol{\omega}\times\boldsymbol{e}_i\right)\right]^{\mathrm{T}}=$$
$$=\left(S\left(\boldsymbol{e}_i\right)S\left(\boldsymbol{e}_i\right)\boldsymbol{\omega}\right)^{\mathrm{T}}=\boldsymbol{\omega}^{\mathrm{T}}S\left(\boldsymbol{e}_i\right)S\left(\boldsymbol{e}_i\right). \tag{20b}$$

From Eq. (20b), we obtain:

$$\begin{bmatrix}\boldsymbol{0}_{1\times3} & \left(\dot{\boldsymbol{e}}_i\times\boldsymbol{\varsigma}_i\right)^{\mathrm{T}}\end{bmatrix}=\boldsymbol{V}^{\mathrm{T}}\begin{bmatrix}\boldsymbol{0}_{3\times3} & \boldsymbol{0}_{3\times3}\\ \boldsymbol{0}_{3\times3} & S\left(\boldsymbol{e}_i\right)S\left(\boldsymbol{\varsigma}_i\right)\end{bmatrix}=\boldsymbol{V}^{\mathrm{T}}\boldsymbol{H}_i,$$
$$\boldsymbol{H}_i=\begin{bmatrix}\boldsymbol{0}_{3\times3} & \boldsymbol{0}_{3\times3}\\ \boldsymbol{0}_{3\times3} & S\left(\boldsymbol{e}_i\right)S\left(\boldsymbol{\varsigma}_i\right)\end{bmatrix}_{6\times6},\quad (i=1,2,3). \tag{20c}$$

By differentiation of Eq. (13b) with respect to time, the acceleration $\boldsymbol{a}_{li}$ along the i^{th} horizontal leg is derived as below:

$$a_{li}=\begin{bmatrix}\boldsymbol{\delta}_i^{\mathrm{T}} & \left(\boldsymbol{e}_i\times\boldsymbol{\delta}_i\right)^{\mathrm{T}}\end{bmatrix}\boldsymbol{A}+$$
$$+\begin{bmatrix}\dot{\boldsymbol{\delta}}_i^{\mathrm{T}} & \left(\dot{\boldsymbol{e}}_i\times\boldsymbol{\delta}_i+\boldsymbol{e}_i\times\dot{\boldsymbol{\delta}}_i\right)^{\mathrm{T}}\end{bmatrix}\boldsymbol{V}. \tag{21a}$$

The derivative of the unit vector $\boldsymbol{\delta}_i$ along the horizontal legs l_i can be expressed as:

$$\dot{\boldsymbol{\delta}}_i=\frac{\boldsymbol{v}_{li}}{l_i}-\frac{v_{li}\boldsymbol{\delta}_i}{l_i}=\frac{1}{l_i}\begin{bmatrix}-S(\boldsymbol{\delta}_i)^2 & S(\boldsymbol{\delta}_i)^2S(\boldsymbol{e}_i)\end{bmatrix}\boldsymbol{V}, \tag{21b}$$

where,

$$v_{li}\boldsymbol{\delta}_i=\left(\begin{bmatrix}\boldsymbol{\delta}_i^{\mathrm{T}} & \left(\boldsymbol{e}_i\times\boldsymbol{\delta}_i\right)^{\mathrm{T}}\end{bmatrix}\boldsymbol{V}\right)\boldsymbol{\delta}_i=$$
$$=\left(\begin{bmatrix}\boldsymbol{\delta}_i\boldsymbol{\delta}_i^{\mathrm{T}} & -\boldsymbol{\delta}_i\boldsymbol{\delta}_i^{\mathrm{T}}S\left(\boldsymbol{e}_i\right)\end{bmatrix}\right)\boldsymbol{V}. \tag{21c}$$

From Eq. (21b), the equation can be shown as:

$$\begin{bmatrix}\dot{\boldsymbol{\delta}}_i^{\mathrm{T}} & \boldsymbol{0}_{1\times3}\end{bmatrix}=\frac{1}{l_i}\boldsymbol{V}^{\mathrm{T}}\begin{bmatrix}-S\left(\boldsymbol{\delta}_i\right)^2 & \boldsymbol{0}_{3\times3}\\ -S\left(\boldsymbol{e}_i\right)S\left(\boldsymbol{\delta}_i\right)^2 & \boldsymbol{0}_{3\times3}\end{bmatrix}. \tag{21d}$$

Similarly, the equation can be obtained as:

$$\left(\dot{\boldsymbol{e}}_i\times\boldsymbol{\delta}_i\right)^{\mathrm{T}}=\left[-S\left(\boldsymbol{\delta}_i\right)\left(\boldsymbol{\omega}\times\boldsymbol{e}_i\right)\right]^{\mathrm{T}}=$$
$$=\left(S\left(\boldsymbol{\delta}_i\right)S\left(\boldsymbol{e}_i\right)\boldsymbol{\omega}\right)^{\mathrm{T}}=\boldsymbol{\omega}^{\mathrm{T}}S\left(\boldsymbol{e}_i\right)S\left(\boldsymbol{\delta}_i\right),$$
$$\left(\boldsymbol{e}_i\times\dot{\boldsymbol{\delta}}_i\right)^{\mathrm{T}}=\left[S\left(\boldsymbol{e}_i\right)\dot{\boldsymbol{\delta}}_i\right]^{\mathrm{T}}=-\dot{\boldsymbol{\delta}}_i^{\mathrm{T}}S\left(\boldsymbol{e}_i\right). \tag{21e}$$

From Eq. (21e), the equation is deduced as:

$$\begin{bmatrix}\boldsymbol{0}_{1\times3} & \left(\dot{\boldsymbol{e}}_i\times\boldsymbol{\delta}_i\right)^{\mathrm{T}}\end{bmatrix}=\boldsymbol{V}^{\mathrm{T}}\begin{bmatrix}\boldsymbol{0}_{3\times3} & \boldsymbol{0}_{3\times3}\\ \boldsymbol{0}_{3\times3} & S\left(\boldsymbol{e}_i\right)S\left(\boldsymbol{\delta}_i\right)\end{bmatrix},$$
$$\begin{bmatrix}\boldsymbol{0}_{1\times3} & \left(\boldsymbol{e}_i\times\dot{\boldsymbol{\delta}}_i\right)^{\mathrm{T}}\end{bmatrix}=\frac{1}{l_i}\boldsymbol{V}^{\mathrm{T}}\begin{bmatrix}\boldsymbol{0}_{3\times3} & S\left(\boldsymbol{\delta}_i\right)^2S\left(\boldsymbol{e}_i\right)\\ \boldsymbol{0}_{3\times3} & S\left(\boldsymbol{e}_i\right)S\left(\boldsymbol{\delta}_i\right)^2S\left(\boldsymbol{e}_i\right)\end{bmatrix}. \tag{21f}$$

Integrating Eqs. (21d) and (21f), we get the following equation:

$$\begin{bmatrix}\dot{\boldsymbol{\delta}}_i^{\mathrm{T}} & \left(\dot{\boldsymbol{e}}_i\times\boldsymbol{\delta}_i+\boldsymbol{e}_i\times\dot{\boldsymbol{\delta}}_i\right)^{\mathrm{T}}\end{bmatrix}=\boldsymbol{V}^{\mathrm{T}}\boldsymbol{H}_i,$$
$$\boldsymbol{H}_i=\frac{1}{l_i}\begin{bmatrix}-S(\boldsymbol{\delta}_i)^2 & S(\boldsymbol{\delta}_i)^2S(\boldsymbol{e}_i)\\ -S(\boldsymbol{e}_i)S(\boldsymbol{\delta}_i)^2 & l_iS(\boldsymbol{e}_i)S(\boldsymbol{\delta}_i)+S(\boldsymbol{e}_i)S(\boldsymbol{\delta}_i)^2S(\boldsymbol{e}_i)\end{bmatrix}_{6\times6},$$
$$(i=4,\ 5,\ 6). \tag{21g}$$

By substituting Eqs. (20c) and (21g) into Eqs. (20a) and (21a) respectively, an inverse acceleration $\boldsymbol{a}_{in}$, a forward acceleration $\boldsymbol{A}$, and a Hessian matrix $\boldsymbol{H}$ are derived as:

$$\boldsymbol{a}_{in}=\boldsymbol{J}\boldsymbol{A}+\boldsymbol{V}^{\mathrm{T}}\boldsymbol{H}\boldsymbol{V},\ \ \boldsymbol{A}=\boldsymbol{J}^{-1}\left(\boldsymbol{a}_{in}-\boldsymbol{V}^{\mathrm{T}}\boldsymbol{H}\boldsymbol{V}\right),$$
$$\boldsymbol{a}_{in}=\begin{bmatrix}a_{h1} & a_{h2} & a_{h3} & a_{l1} & a_{l2} & a_{l3}\end{bmatrix}^{\mathrm{T}},$$
$$\boldsymbol{H}=\begin{bmatrix}\boldsymbol{H}_1 & \boldsymbol{H}_2 & \boldsymbol{H}_3 & \boldsymbol{H}_4 & \boldsymbol{H}_5 & \boldsymbol{H}_6\end{bmatrix}^{\mathrm{T}}. \tag{22}$$

At this point, the kinematic model of the 3CPS parallel manipulator is established.

3 NUMERICAL SIMULATIONS AND EXPERIMENTAL VERIFICATION

3.1 Numerical Simulations

The designed structural parameters of the developed active adjusting platform are noted in Table 1 and the set variations of the six independent pose parameters of the moving platform (X_o, Y_o, Z_o, α, β, γ) are shown in Fig. 2. The corresponding Rodrigues parameters Φ_1, Φ_2 and Φ_3 vary continuously with time. Following these variations, a numerical simulation of the inverse kinematics is implemented using the Matlab program at 0.01 s intervals.

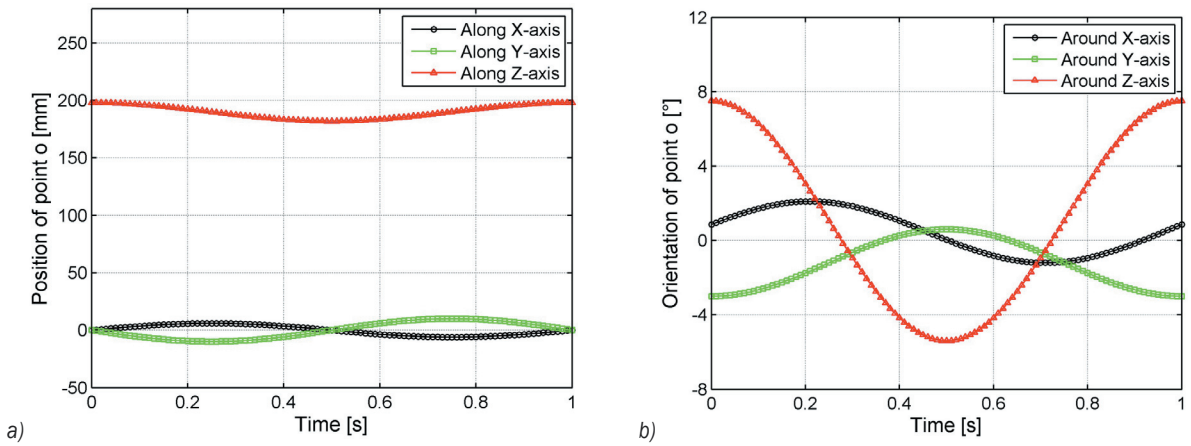

Fig. 2. *Variations in the six pose parameters; a) position variations (X_o, Y_o, Z_o), and b) orientation variations (α, β, γ)*

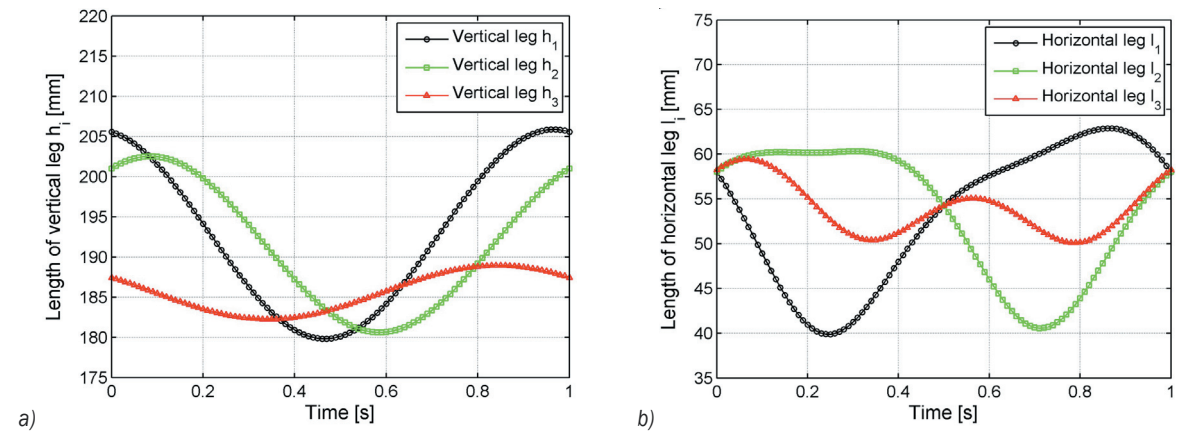

Fig. 3. *Length variations in the driving legs; a) length variations in the vertical legs, and b) length variations in the horizontal legs*

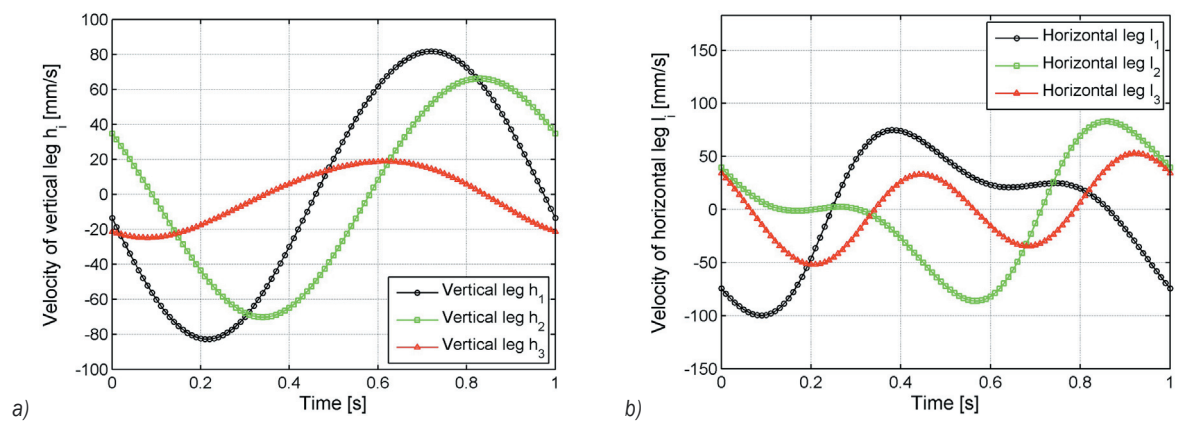

Fig. 4. *Velocity variations in the driving legs; a) velocity variations in the vertical legs, and b) velocity variations in the horizontal legs*

The length variations in the vertical legs and in the horizontal legs are shown in Fig. 3. The length ranges of the active legs are all within the design limits. Combined with the structural parameters, the driving legs have no structural interference during movement. The length variations of active legs approximate to the simple harmonic curves and this characteristic benefits the control of the moving platform.

The velocity variations of the active legs according to Fig. 3 are shown in Fig. 4, and the corresponding acceleration variations are shown in Fig. 5. Fig. 4a and Fig. 5a indicate that the vertical

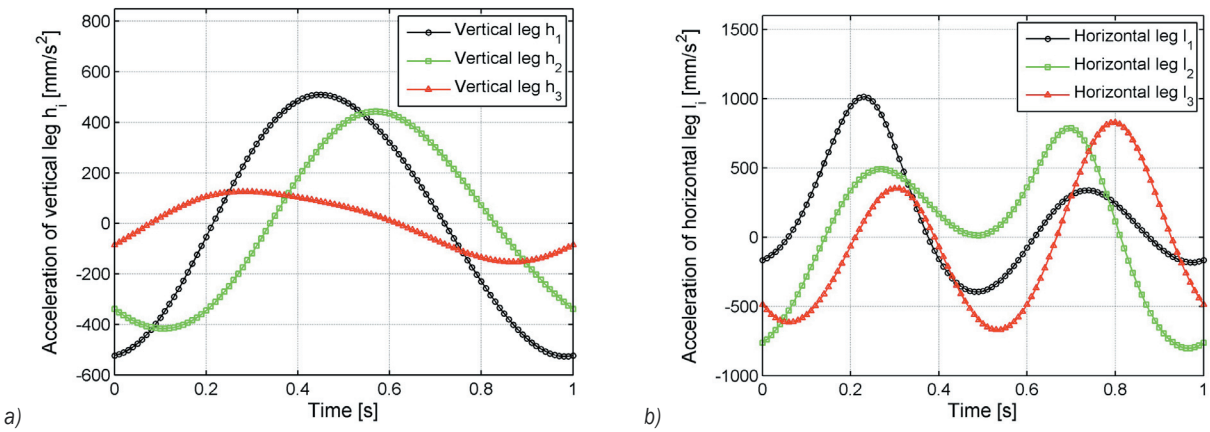

Fig. 5. *Acceleration variations in the driving legs; a) acceleration variations in the vertical legs, and b) acceleration variations in the horizontal legs*

legs h_1 and h_2 have approximately the same velocity and acceleration variation ranges, while that of leg h_3 is slightly smaller than the other two. Fig. 5 indicates that all three horizontal legs have large variation ranges of acceleration compared to the vertical legs. The large variation ranges in the acceleration increase the demand for the dynamic performance of the driving motors, especially for that of the horizontal legs. The curves of velocities and accelerations vary smoothly and have no abrupt change points. Therefore, there is no rigid shock in the motion of the moving platform. This is important for the dynamic behaviour of the moving platform.

Table 1. *Main parameters of 3CPS parallel manipulator*

Structural parameters of the manipulator	Value [mm]
Installation Radius of *B* (*E*)	250
Installation Radius of *m* (*e*)	200
Minimum length of vertical legs	170
Maximum length of vertical legs	210
Minimum length of horizontal legs	30
Maximum length of horizontal legs	250

3.2 Experimental Verification

Photogrammetric measurement based on computer vision and image processing technology has become an excellent measurement method. It has been widely used in the industrial and scientific fields, such as in industrial inspection, reverse engineering, and robot vision systems [20]. In order to verify the correctness of the theoretical kinematics model, the photogrammetric pose measurement method with a single camera is used to measure the positions and orientations of the moving platform in this paper [21] and [22]. Single camera solutions are of interest in restricted applications, such as the restrictions in terms of costs, synchronisation demands or spatial observation conditions.

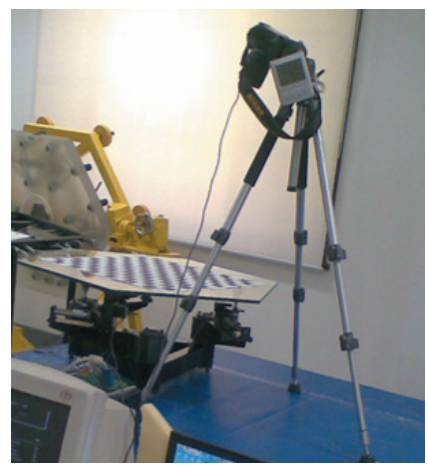

Fig. 6. *Test environment for photogrammetric measurement*

The test environment for photogrammetric measurement is shown in Fig. 6. The moving platform of the 3CPS parallel manipulator is made of a hexagonal glass plate, which is covered by a black and white grid pattern. The pose is measured by using a NIKON D80 camera after calibrating using free software calib-for-matlab. Considering the image size and processing speed, a medium image resolution (2896×1944 pixels) is used in the experiment. In addition, the computer is used to control the camera shutter and the ambient temperature is monitored to ensure the stability of the measuring process.

The process for testing the kinematic performance as well as concrete steps for photogrammetry to measure a specific pose are listed as follows: a) connect all the components of the developed parallel manipulator as shown in Fig. 1; b) post the grid pattern, align with the center of glass plate, and check the motion of the motors; c) connect the camera to the computer, sample several different poses of the grid pattern and calibrate camera; d) obtain the pose of the moving platform at a fixed time according to the designed trajectory and sampled frequency; e) substitute the pose into the theoretical kinematic model and calculate the corresponding leg length; f) control the motor according to the calculated leg length, use a height gauge, and vernier caliper to measure the length of the legs and shoot the grid paper at the fixed pose; g) calculate the poses of the moving platform by using the calibrated parameters of the camera.

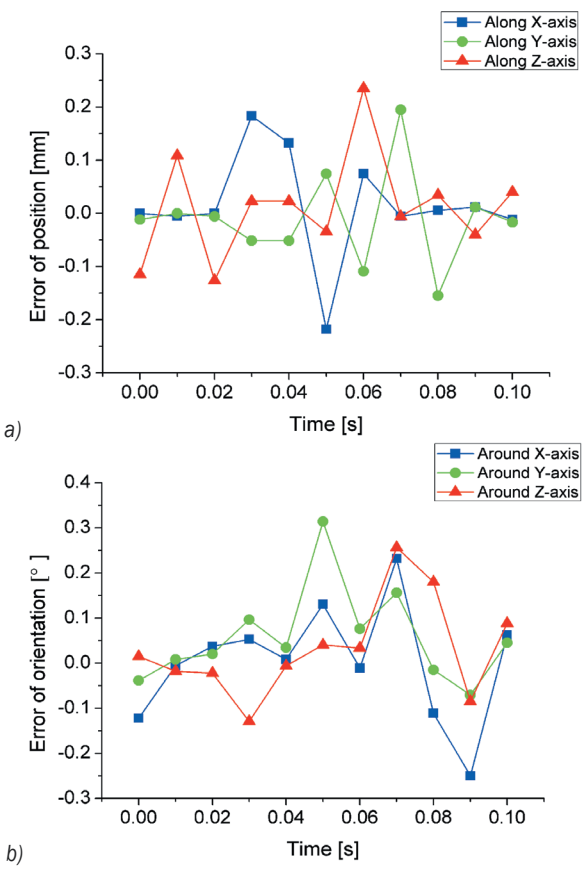

Fig. 7. *Error between designed trajectories and experimental results; a) error of position, and b) error of orientation*

In order to get a smooth curve, we selected sampling time at 0.01 s. Thus, we obtain 100 groups of data within a period of 1 s during the simulation process. The purpose of the experiment is to verify the theoretical kinematics model in this paper. Considering the efficiency and cost required for the measurement, it does not make sense to test one by one and cover the whole range of calculations. To compare the experimental results with the designed trajectories intuitively, only the errors of position and orientation between two groups from 0 to 0.1 s with a sampling time at 0.01 s are shown in Fig.7. Therefore, there are 11 groups of data in the error sequence. Errors exist between the designed trajectories and the experimental results. Fig. 7 shows that the position error is about 0.2 mm and the orientation error is about 0.3°. An initial analysis of causes of the errors is as follows:

1) Errors of measurement tool: The grid pattern is printed using an inkjet printer and the paper is not flat due to the infiltration of ink. The sizes of the grid are also different. After measurement, the average size of the grid is 40.07×40.23 mm. However, a nominal size 40.00×40.00 mm is used in the simulation process. There are also differences between the coordinate system of the grid pattern and the moving platform due to the placement error.

2) Differences between the physical prototype and the simulation model: Manufacturing and assembly errors, which are inevitable, exist in the physical prototype, while nominal ideal size is used in the simulation process. Moreover, the control system has no automatic feedback.

3) Influences due to the environment: During the experiment, changes in ambient temperature, vibration and even light have a great impact on camera calibration and measurement accuracy.

All the errors mentioned above will cause pose errors of the moving platform in the photogrammetric measurement. However, considering the errors of the measurement tools, the differences between the physical prototype and the simulation model, as well as environmental influences, the comparison results in Fig. 7 show that the theoretical value and the experimental results agree very well in a generally manner and verify the correctness of the kinematics model.

4 CONCLUSIONS

A prototype of the 3CPS active adjusting platform for a segment mirror with 6 DOFs has been established. This prototype has partial DOF-decoupling motion characteristics and the mobility properties of the manipulator are analysed. The kinematics of the manipulator is studied in depth. The derived

final formulae for solving the inverse/forward displacement, velocity, and acceleration of the 6 DOFs parallel active adjusting platform are quite simple. According to the topological structure, the characteristics of the manipulator and the designed trajectories of the moving platform, the lengths, velocities, and accelerations of the six driving legs are constructed based on inverse kinematics by numerical simulation. Meanwhile, the analytic results of this parallel manipulator are verified by the experiments in which the pose of moving platform is measured using a photogrammetric method. Though errors exist between the designed trajectories and the experimental results, the experimental results prove the correctness of the kinematics model overall.

5 NOMENCLATURE

$\{m\}$	relative coordinate system *o-xyz* fixed on *m*
$\{B\}$	absolute coordinate system *O-XYZ* fixed on *B*
D_o	rotation transformation matrix from $\{m\}$ to $\{B\}$
h_i (i=1,2,3)	active vertical leg and its length
l_i (i=1,2,3)	active horizontal leg and its length
O	center point of *B*
o	center point of *m*
a_i (i=1,2,3)	attachment points of *m* with surrounding legs
A_i (i=1,2,3)	attachment points of *B* with surrounding legs
D_i (i=1,2,3)	end point of the vertical legs
e	distance from a_i to o
E	distance from A_i to O
$\boldsymbol{\varsigma}$ (i=1,2,3)	unit vector of h_i
$\boldsymbol{\delta}_i$ (i=1,2,3)	unit vector of l_i
$\boldsymbol{u}_o$, $\boldsymbol{v}_o$, $\boldsymbol{w}_o$	unit vectors of *x, y* and *z*
$\boldsymbol{v}_{hi}$ (i=1,2,3)	velocity of active vertical leg h_i
$\boldsymbol{v}_{li}$ (i=1,2,3)	velocity of active horizontal leg l_i
$\boldsymbol{V}$	the forward general velocity, $\boldsymbol{V}=[\boldsymbol{v}\ \boldsymbol{\omega}]^{\mathrm{T}}$
$\boldsymbol{J}$	Jacobian matrix
ω_{Ci}(i=1,2,3)	angular velocities of vertical legs
$\boldsymbol{a}_{hi}$ (i=1,2,3)	acceleration of active vertical leg h_i
$\boldsymbol{a}_{li}$ (i=1,2,3)	acceleration of active horizontal leg l_i
$\boldsymbol{A}$	the forward general acceleration, $\boldsymbol{A}=[\boldsymbol{a}\ \boldsymbol{\varepsilon}]^{\mathrm{T}}$
$\boldsymbol{H}$	Hessian matrix

6 ACKNOWLEDGMENTS

Financial support for this work, provided by the National Natural Science Foundation of China (Grant No. 51275512), the Fundamental Research Funds for the Central Universities (Grant No. 2012LWB36), and the Priority Academic Program Development of Jiangsu Higher Education Institutions, is gratefully acknowledged.

7 REFERENCES

[1] Chang, J., Cao, J., Cheng, D., Feng, S., Jiang, H. (2011). The system design and assemble for the high resolution telescope system with segmented aperture. *Optik-International Journal for Light and Electron Optics*, vol. 122, no. 18, p. 1628-1632, DOI:10.1016/j.ijleo.2010.10.015.

[2] Preumont, A., Bastaits, R., Rodrigues, G. (2009). Scale effects in active optics of large segmented mirrors. *Mechatronics*, vol. 19, no. 8, p. 1286-1293, DOI:10.1016/j.mechatronics.2009.08.005.

[3] Shore, P., Cunninghamb, C., DeBra, D., Evans, C., Hough, J., Gilmozzi, R., Kunzmann, H., Morantz, P., Tonnellier, X. (2010). Precision engineering for astronomy and gravity science. *CIRP Annals - Manufacturing Technology*, vol. 59, no. 2, p. 694-716, DOI:10.1016/j.cirp.2010.05.003.

[4] Cheng, G., Yu, J., Ge, S., Zhang, S. (2011). Workspace analysis of 3SPS+1PS bionic parallel test platform for hip joint simulator. *Proceeding of the Institution of Mechanical Part C - Journal of Mechanical Engineering Science*, vol. 225, no. 9, p. 2216-2231, DOI:10.1177/0954406211404864.

[5] Cheng, G., Gu, W., Yu, J., Tang, P. (2011). Overall structure calibration of 3-UCR parallel manipulator based on quaternion method. *Strojniški vestnik - Journal of Mechanical Engineering*, vol. 57, no. 10, p. 719-729, DOI:10.5545/sv-jme.2010.167.

[6] Harib, K., Sharif Ullah, A., Hammami, A. (2007). A hexapod-based machine tool with hybrid structure: Kinematic analysis and trajectory planning. *International Journal of Machine Tools and Manufacture*, vol. 47, no. 9, p. 1426-1432, DOI:10.1016/j.ijmachtools.2006.09.021.

[7] Terrier, M., Dugas, A., Hascoet, J. (2004). Qualification of parallel kinematics machines in high-speed milling on free form surfaces. *International Journal of Machine Tools and Manufacture*, vol. 44, no. 7-8, p. 865-877, DOI:10.1016/j.ijmachtools.2003.11.003.

[8] Chanala, H., Duca, E., Raya, P., Hascoe, J. (2007). A new approach for the geometrical calibration of parallel kinematics machines tools based on the machining of a dedicated part. *International Journal of Machine Tools and Manufacture*, vol. 47, no. 7-8, p. 1151-1163, DOI:10.1016/j.ijmachtools.2006.09.006.

[9] Riccardi, A., Xompero, M., Zanotti, D., Busoni, L. (2008). The adaptive secondary mirror for the Large Binocular Telescope: results of acceptance laboratory test. *Proceedings of the SPIE*, vol. 6, p. 7015-7037, DOI:10.1117/12.790527.

[10] Zago, L., Genequand, P., Moerschell, J. (1998). Extremely compact secondary mirror unit for the SOFIA telescope capable of 6-degree-of-freedom alignment plus chopping. *Proceedings of the SPIE*, vol. 3352, p. 666-674, DOI:10.1117/12.319276.

[11] Schipani, P., Marty, L. (2006). Stewart platform kinematics and secondary mirror aberration control. *Proceedings of the SPIE*, vol. 6273, p. 1026-1237, DOI:10.1117/12.670537.

[12] Cheng, G., Yu, J., Gu, W. (2012). Kinematic analysis of 3SPS+1PS bionic parallel test platform for hip joint simulator based on unit quaternion. *Robotics and Computer Integrated Manufacturing*, vol. 28, no. 2, p. 257-264, DOI:10.1016/j.rcim.2011.09.007.

[13] Lu, Y., Shi, Y., Huang, Z., Yu, J., Li, S., Tian, X. (2009). Kinematics/statics of a 4-DOF over-constrained parallel manipulator with 3 legs. *Mechanism and Machine Theory*, vol. 44, no. 8, p. 1497-1506, DOI:10.1016/j.mechmachtheory.2008.12.001.

[14] Gallardoa, J., Lessoa, R., Rico, J., Alici, G. (2011). The kinematics of modular spatial hyper-redundant manipulators formed from RPS-type limbs. *Robotics and Autonomous Systems*, vol. 59, no. 1, p. 12-21, DOI:10.1016/j.robot.2010.09.005.

[15] Cui, H., Zhu, Z., Gan, Z., Brogardh, T. (2005). Kinematic analysis and error modeling of TAU parallel robot. *Robotics and Computer Integrated Manufacturing*, vol. 21, no. 6, p. 497-505, DOI:10.1016/j.rcim.2004.07.018.

[16] Varedi, S., Daniali, H., Ganji, D. (2009). Kinematics of an offset 3-UPU translational parallel manipulator by the homotopy continuation method. *Nonlinear Analysis: Real World Applications*, vol. 10, no. 3, p. 1767-1774, DOI:10.1016/j.nonrwa.2008.02.014.

[17] Zhang, Y., Mu, D. (2010). New concept and new theory of mobility calculation for multi-loop mechanisms. *Science China Technology Science*, vol. 53, no. 6, p. 1598-1604, DOI:10.1007/s11431-010-3100-y.

[18] Zhou, J., Miao, Y., Wang, M. (2004). Attitude representation using Rodrigues parameter. *Journal of Astronautics*, vol. 25, no. 5, p. 514-519. (in Chinese)

[19] Craig, J. (2005). *Introduction to robotics: mechanics and control*, 3rd ed. Prentice Hall/Pearson Press, New York.

[20] Papa, G., Torkar, D. (2009) Visual control of an industrial robot manipulator: accuracy estimation. *Strojniški vestnik - Journal of Mechanical Engineering*, vol. 55, no. 12, p. 781-787.

[21] Li, H., Yang, D., Zhai, C. (2010). Research on the pose measurement of a 6-DOF platform using a single camera. *Optical Technique*, vol. 36, no. 3, p. 344-349. (in Chinese)

[22] Luhmann, T. (2009). Precision potential of photogrammetric 6 DOF pose estimation with a single camera. *ISPRS Journal of Photogrammetry and Remote Sensing*, vol. 64, no. 3, p. 275-284, DOI:10.1016/j.isprsjprs.2009.01.002.